Your MICCAI Paper Title

Anonymized Authors

Anonymized Affiliations
email@anonymized.com

Abstract. Automated analysis of spinal radiographs is critical to early diagnosis but is currently limited by severe class imbalance and the visual subtlety of lesions. This work introduces DERNet—an ensemble of DenseNet121, EfficientNetV2-S, and ResNet50—for highly sensitive classification, coupled with a YOLO11-L model for precise lesion detection. Our proposed method utilizes architectural diversity to overcome the sensitivity-specificity trade-off, along with a CSP-Darknet backbone to effectively capture the fine features of minute pathologies. The proposed framework is validated on the VinDr-SpineXR benchmark, yielding state-of-the-art AUROC of 91.03% and detection mAP@0.5 on 40.10%. In addition to the technical contributions, the authors address the translational challenge with the development of a functional web-based interface that can process various image formats, thereby facilitating the practical application of the proposed framework. All the code associated with this study is available at: GitHub

Keywords: Spinal Lesion · DERNet · Class Imbalance · Clinical Deployment.

1 Introduction

The spinal column is central to mechanical integrity and serves as the primary shield for the central nervous system [18]. However, it remains highly susceptible to a spectrum of pathologies, ranging from degenerative diseases, such as disc space narrowing and osteophytes, to structural anomalies including spondylolisthesis and foraminal stenosis [9]. The absence of timely diagnosis frequently precipitates severe sequelae, including radiculopathy and permanent neurological deficit [11,5].

While conventional radiography (X-ray) remains the gold standard for initial screening due to cost-efficiency and accessibility [12,9], manual interpretation is labor-intensive and prone to inter-observer variability caused by complex anatomical superposition [7]. Consequently, the development of high-precision Computer-Aided Diagnosis (CAD) systems has become imperative to augment clinical decision-making [1].

To address these challenges, we present a unified, end-to-end framework designed for both diagnostic accuracy and translational utility. Our main contributions are threefold:

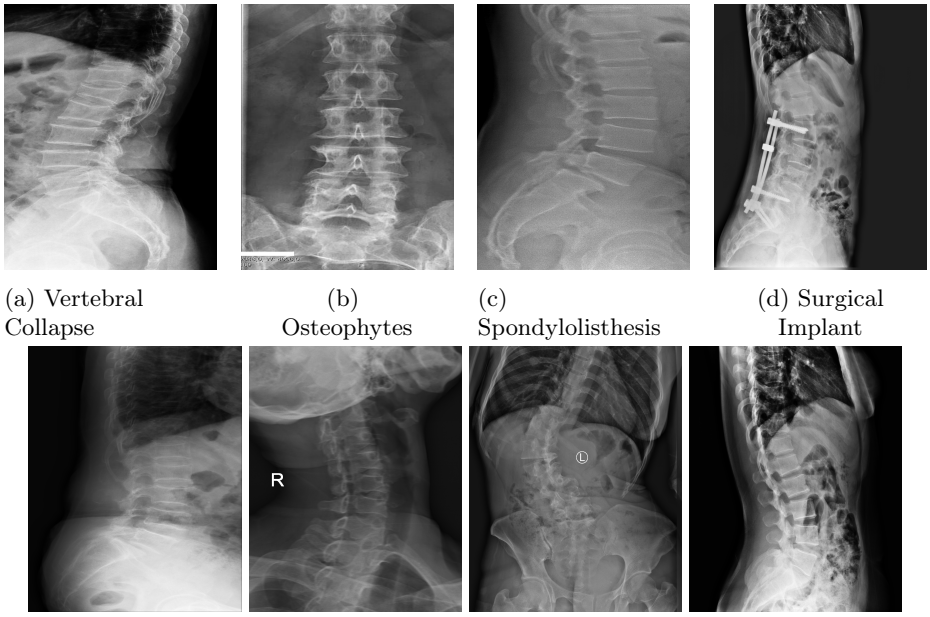

(a) Vertebral Collapse (b) Osteophytes (c) Spondylolisthesis (d) Surgical Implant

(e) Disc Space Narrowing (f) Foraminal Stenosis (g) Other Lession (h) Normal

Fig. 1: Examples of detected spinal lesions in X-ray images. The figure highlights four distinct pathologies: (a) Vertebral Collapse, (b) Osteophytes, (c) Spondylolisthesis, (d) Surgical Implants, (e) Disc Space Narrowing, (f) Foraminal Stenosis, (g) Other Lession and (h) Normal.

1. **Robust Triage (DERNet):** We propose a triage mechanism that synergizes DenseNet121 [4], EfficientNetV2-S [17], and ResNet50 [3] via a weighted soft-voting technique. This approach mitigates individual architectural biases to strictly filter normal cases, thereby optimizing clinical workflow efficiency.
2. **High-Precision Localization:** We introduce a customized YOLO11-L architecture explicitly optimized for extreme class imbalance and small object detection. This module effectively resolves subtle pathologies, such as Foraminal Stenosis, which are frequently missed by state-of-the-art baselines.
3. **Clinical Translation:** Bridging the gap between research and practice, we provide a deployment-ready web interface integrated with Automated Outlier Rejection, ensuring model reliability in real-world clinical environments.

2 Related Work

Automated spinal analysis has evolved from manual feature extraction to Deep Learning (DL) paradigms [14]. Nguyen et al. established the foundational *VinDr-*

SpineXR [9] benchmark; however, their ResNet-18 baseline exhibited limited sensitivity, a critical risk for clinical triage. Recent architectures (2024–2025) have attempted to address this. Khan et al. [6] proposed *HealNNet* for screening, while others explored Transformer-based methods and ensembles. Despite these advancements, such methods often plateau in accuracy or incur high computational costs when handling radiographic noise. Our work overcomes these limitations by synergizing feature reuse (DenseNet), parameter efficiency (EfficientNet), and residual learning (ResNet) into a cohesive weighted ensemble.

In lesion localization, performance is constrained by extreme class imbalance (46.9:1) and minute object scales. Traditional detectors like Faster R-CNN [13] and Sparse R-CNN [15] frequently miss subtle pathologies. While Guo et al. [2] introduced edge-guidance (*EGCA-Net*) to sharpen boundaries, their approach remains susceptible to complex background artifacts. Similarly, recent YOLO applications [16] have largely been restricted to fracture detection or CT modalities. The authors advance this domain by customizing the YOLO11-L architecture specifically for multi-class X-ray imbalance, bridging the gap between research models and clinical deployment.

3 Methodology

Our framework addresses the dual challenges of spinal pathology screening and fine-grained localization through a unified, end-to-end pipeline. The system integrates a probabilistic DERNet for high-sensitivity triage and a specialized single-stage detector optimized for minute anatomical anomalies, as illustrated in Fig. 2.

3.1 Dataset and Adaptive Preprocessing

We utilized the *VinDr-SpineXR* dataset [10], comprising $N = 8,389$ spinal radiographs. The dataset exhibits a severe class imbalance ratio of 46.9:1, where majority classes (e.g., Osteophytes) dominate critical minority classes (e.g., Vertebral Collapse).

To mitigate high variance in X-ray exposure, we employ Contrast Limited Adaptive Histogram Equalization (CLAHE). Let $I(i, j)$ denote the pixel intensity at coordinates (i, j). The enhanced intensity $I'(i, j)$ is computed by mapping the local Cumulative Distribution Function (CDF) within a contextual region Ω_k, as defined in Eq. 1:

$$I'(i,j) = \beta \left(\frac{CDF_{\Omega_k}(I(i,j)) - CDF_{min}}{M \cdot N - CDF_{min}} \right), \tag{1}$$

where $M \cdot N$ is the cardinality of region Ω_k, and β is the dynamic range scaling factor. We set the clip limit $\tau = 2.0$ to prevent noise amplification in homogeneous bone structures.

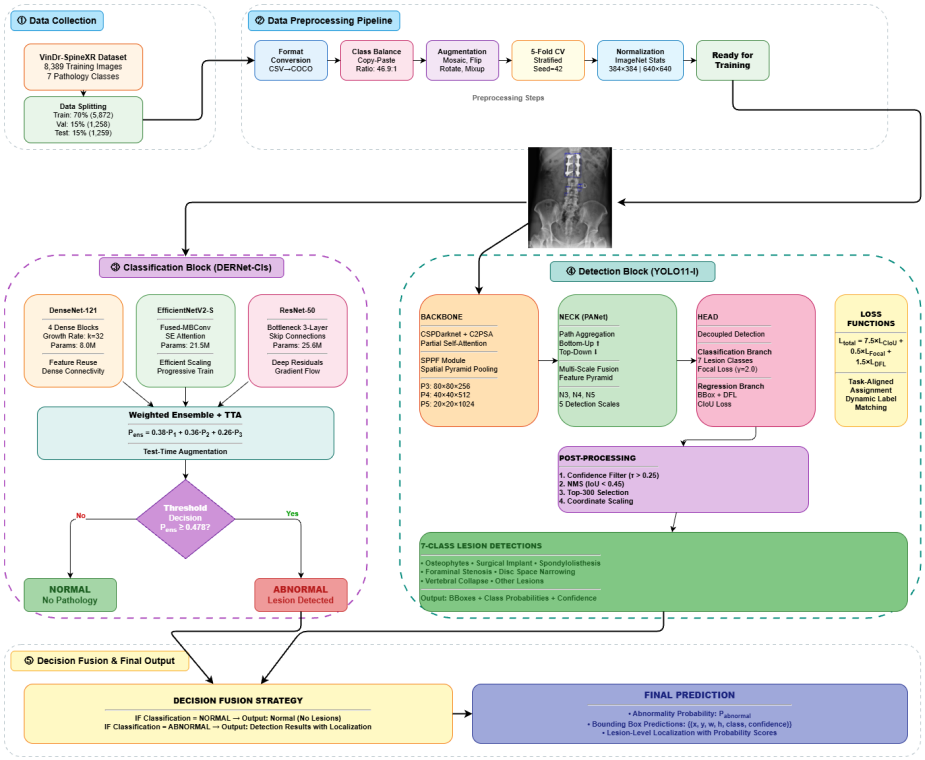

Fig. 2: Architectural Overview. The pipeline consists of (A) Adaptive Preprocessing via CLAHE, (B) A Probabilistic DERNet for binary triage, and (C) A YOLO11-L Detection Network with optimized Path Aggregation for small-lesion localization.

3.2 Probabilistic DERNet Classification

To optimize the filtration of normal studies, we construct a heterogeneous ensemble, DERNet, comprising DenseNet121, EfficientNetV2-S, and ResNet50. This combination synergizes feature reuse, parameter efficiency, and residual gradient flow. Given an input $\mathbf{x}$, each backbone f_{θ_m} maps latent embeddings to a posterior $P(y = c|\mathbf{x}; \theta_m)$. The final prediction $\hat{y}$ employs a Weighted Soft-Voting strategy (Eq. 2) to marginalize predictive uncertainty:

$$\hat{y} = _{c\in\{0,1\}} \left(\sum_{m=1}^{|\mathcal{E}|} \omega_m \cdot P(y = c|\mathbf{x}; \theta_m) \right), \tag{2}$$

subject to $\sum \omega_m = 1$. The weights $\mathbf{\Omega} = [0.42, 0.32, 0.26]$ were empirically optimized to prioritize DenseNet's feature propagation for subtle spinal textures.

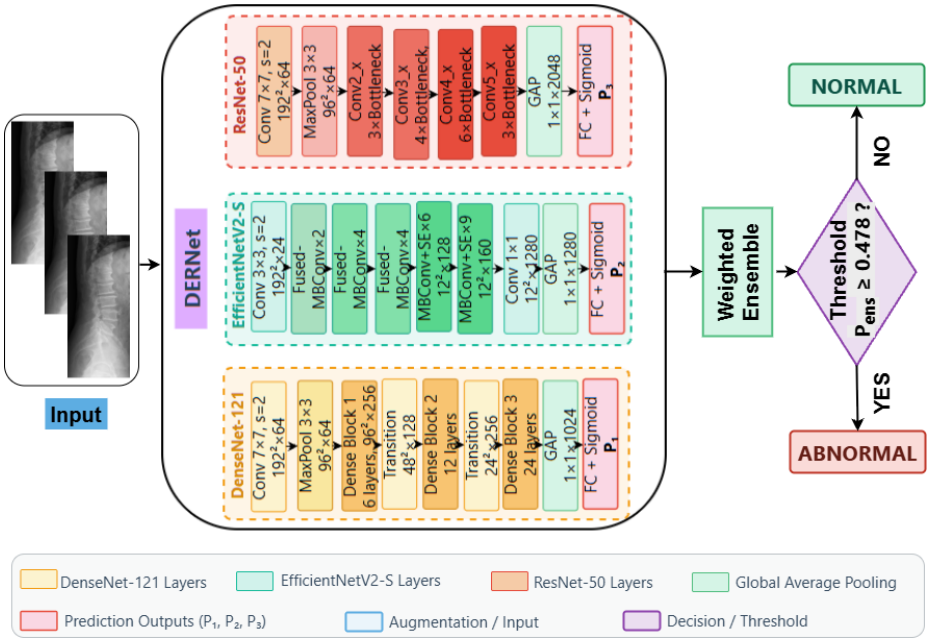

Fig. 3: Schematic of the DERNet Architecture. The framework fuses DenseNet121, EfficientNetV2-S, and ResNet50 via a weighted soft-voting mechanism to distinguish normal vs. abnormal studies with high sensitivity.

3.3 Fine-Grained Localization (YOLO11-L)

For lesion localization, we deploy YOLO11-L, explicitly optimized for the "small object" problem (lesion area $< 1\%$ of FOV). Unlike previous iterations, our architecture incorporates a Cross-Stage Partial (CSP) Darknet backbone enhanced with C2PSA (CSP with Partial Self-Attention) blocks. The attention mechanism within the C2PSA block enhances feature discriminability by computing the scaled dot-product attention as shown in Eq. 3:

$$\text{Attention}(Q, K, V) = \text{softmax}\left(\frac{QK^T}{\sqrt{d_k}}\right)V, \tag{3}$$

where d_k is the scaling factor. Feature fusion is handled by an optimized Path Aggregation Network (PANet), which preserves high-frequency spatial information critical for Foraminal Stenosis detection.

Loss Function Optimization. The network minimizes a composite objective function $\mathcal{L}_{total}$ (Eq. 4), which balances geometric alignment with classification accuracy:

$$\mathcal{L}_{total} = \lambda_{box}\mathcal{L}_{CIoU} + \lambda_{cls}\mathcal{L}_{Focal} + \lambda_{dfl}\mathcal{L}_{DFL}. \tag{4}$$

We configured the loss weights as $\lambda_{box} = 7.5$, $\lambda_{cls} = 0.5$, and $\lambda_{dfl} = 1.5$ to prioritize geometric precision. The components are defined as follows:

Box Regression ($\mathcal{L}_{CIoU}$). To ensure precise localization, we employ the Complete Intersection over Union loss, defined in Eq. 5. This term penalizes the Euclidean distance between center points (ρ) and the aspect ratio variance (v):

$$\mathcal{L}_{CIoU} = 1 - IoU + \frac{\rho^2(\mathbf{b}, \mathbf{b}^{gt})}{c^2} + \alpha v, \tag{5}$$

where c is the diagonal length of the smallest enclosing box covering the two boxes.

Classification ($\mathcal{L}_{Focal}$). To address the extreme foreground-background imbalance inherent in spinal anomaly detection, we utilize Focal Loss (Eq. 6) with a modulating factor $\gamma = 2.0$. This down-weights easy negatives to focus learning on hard misclassified examples:

$$\mathcal{L}_{Focal} = -\alpha_t(1 - p_t)^\gamma \log(p_t). \tag{6}$$

Distribution Focal Loss ($\mathcal{L}_{DFL}$). Finally, we incorporate $\mathcal{L}_{DFL}$ to model bounding box edges as general distributions. This is critical for handling the ambiguous lesion boundaries often observed in subtle pathologies like osteophytes.

Clinical Deployment Interface. To bridge the gap between research and practice, we engineered a web interface capable of processing multi-modal inputs (DICOM, PNG, JPEG). By leveraging ONNX Runtime, the system ensures low-latency inference on standard clinical hardware. As detailed in Algorithm 1, this interface integrates the full pipeline—from triage to localization—delivering real-time automated diagnostic reports to augment radiologist decision-making.

4 Results & Discussions

In this section, we present a comprehensive evaluation of the proposed framework on the VinDr-SpineXR dataset. We first detail the experimental protocols and evaluation metrics, followed by a quantitative analysis of the DERNet classification performance and YOLO11-L localization precision. Finally, we provide qualitative visualizations to demonstrate the model's clinical applicability.

4.1 Experimental Setup

We applied VinDr-SpineXR protocols [9] ($N = 2,078$) with 5-Fold Stratified Cross-Validation. Implementation: PyTorch 2.0.1, NVIDIA RTX 3050 (8GB). Reproducibility: fixed seeds ($seed = 42$) and deterministic algorithms. Training: AdamW optimization. Classification: 60 epochs (Cosine Annealing); YOLO11-L: 55 epochs (Batch 12, Mosaic Augmentation). Time: ≈45h. Validation: Bootstrap resampling ($B = 1000$, 95% CI) and paired t-tests ($p < 0.05$).

Table 1: Adaptive Training & Inference Protocol

Algorithm 1: End-to-End Pipeline Logic

Require: Dataset $\mathcal{D} = \{(x_i, y_i)\}_{i=1}^{N}$, DERNet Ensemble $\mathcal{E}$, Detector $\mathcal{Y}$
Hyperparameters: $\eta = 1e^{-4}$ (LR), $\tau_{mosaic} = 25$ (Augmentation Cutoff)

Phase I: DERNet Optimization
for $m \in \{1, \ldots, 3\}$ **do**
  $\theta_m \leftarrow \theta_{ImageNet}$ // *Transfer Learning Initialization*
  while not converged **do**
    $\mathcal{L}_{CE} \leftarrow -\sum_i [y_i \log(\hat{y}_i) + (1 - y_i) \log(1 - \hat{y}_i)]$
    $\theta_m \leftarrow \theta_m - \eta \nabla_{\theta_m} \mathcal{L}_{CE}$ // *AdamW Update*
  end while
end for

Phase II: Detection with Mosaic Decay
for epoch $t = 1 \rightarrow T_{max}$ **do**
  if $t < \tau_{mosaic}$ **then**
    $x' \leftarrow MosaicAug(x) \sim U(0.3W, 0.7W)$ // *Synth. context*
  else
    $x' \leftarrow x$ // *Disable Mosaic for distribution alignment*
  end if
  Update θ_Y minimizing $\mathcal{L}_{total}$ (Eq. 4)
end for

Phase III: Clinical Inference Logic
Score $\mathcal{S} \leftarrow \sum_{m=1}^{3} \omega_m P_m(x)$
if $\mathcal{S} > \tau_{optimal}$ **then**
  $\mathcal{B} \leftarrow \text{NMS}(\mathcal{Y}(x), \text{IoU}_{thresh} = 0.5)$ // *Filter Overlaps*
  return $\mathcal{B}$
else
  return $\emptyset$ (Normal Study)
end if

4.2 Experimental results

Classification Performance. Table 2 benchmarks our framework against established baselines [9,6]. While individual backbones exhibited distinct biases EfficientNetV2-S favoring specificity (91.12%) versus ResNet50's recall priority—our Weighted Soft-Voting strategy successfully harmonized these representations. Consequently, DERNet achieved a state-of-the-art AUROC of 91.03%, significantly outperforming the VinDr-SpineXR baseline (88.61%) while maintaining a robust clinical equilibrium (Sensitivity: 84.91%, Specificity: 81.68%).

Table 2: Classification performance comparison. Best results are in **bold**.

Method	AUROC (%)	F1 (%)	Sens. (%)	Spec. (%)
EfficientNetV2-S	89.44	79.34	70.80	91.12
ResNet50	88.88	80.15	82.72	78.13
DenseNet121	86.93	79.55	80.39	79.32
VinDr Ensemble [9]	88.61	81.06	83.07	79.32
HealNNet [6]	88.84	81.20	-	-
DERNet	**91.03**	**83.09**	**84.91**	**81.68**

Detection Performance. Table 3 benchmarks the proposed YOLO11-L framework against incumbent models using mean Average Precision (mAP) at an IoU threshold of 0.5. Our architecture establishes a new localization standard, achieving a mAP@0.5 of 40.10% and demonstrating robust efficacy across heterogeneous spinal lesions. Notably, the model excels in fine-grained categories, attaining an AP of 41.40% for Foraminal Stenosis (LT4). These results validate the capacity of the optimized CSP-Darknet backbone to preserve high-frequency anatomical features essential for small-object localization.

Table 3: Comparison results of different methods. The detection performance for each type of spinal lesion is evaluated by AP (%) at 0.5 IoU threshold. Best results are in **bold**.

Method	LT2$^{(*)}$	LT4	LT6	LT8	LT10	LT11	LT13	mAP@0.5
Dino [19]	16.58	22.87	28.53	32.71	59.78	41.28	3.24	29.28
RetinaNet [8]	14.53	25.35	41.67	32.14	65.49	51.85	5.30	28.09
Faster R-CNN [13]	22.66	35.99	49.24	31.68	65.22	51.68	2.16	31.83
Sparse R-CNN [15]	20.09	32.67	48.16	45.32	72.20	49.30	5.41	33.15
VinDr-SpineXR [9]	21.43	27.36	34.78	41.29	62.53	43.39	**4.16**	33.56
EGCA-Net [2]	22.36	29.75	36.73	44.69	66.58	50.41	2.09	36.09
Ours (YOLO11-L)	**26.70**	**41.40**	**40.60**	**54.80**	**74.10**	**51.20**	2.99	**40.10**

$^{(*)}$ LT2, LT4, LT6, LT8, LT10, LT11, LT13 denotes for disc space narrowing, foraminal stenosis, osteophytes, spondylolysthesis, surgical implant, vertebral collapse and other lesions, respectively, following the same indexing in Table 2.

Qualitative Analysis. Fig. 4 validates the clinical relevance of DERNet. LIME (a) confirms the model's focus on *meaningful structures* rather than background artifacts. Grad-CAM (b) ensures *transparent validation*, with heatmaps aligning precisely to pathological lesions. Finally, Segmentation (c) demonstrates superior *anatomical fidelity*, preserving fine details often missed by baseline models.

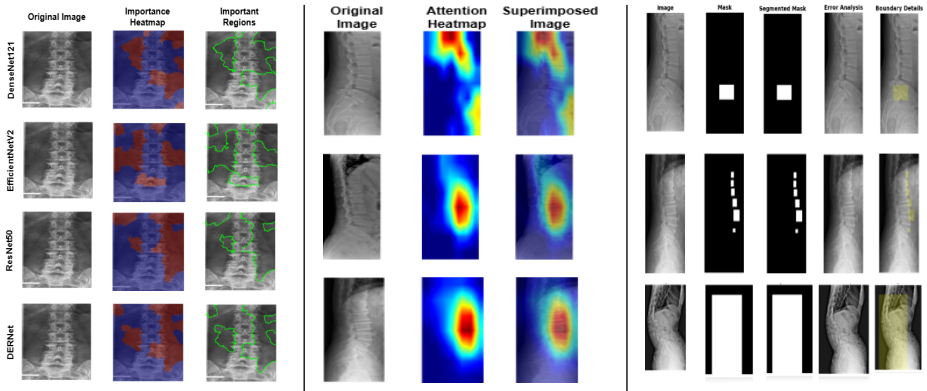

(a) LIME Explainability (b) Grad-CAM Analysis (c) Segmentation Details

Fig. 4: **Performance Evaluation.** (a) **Explainability:** LIME confirms focus on meaningful structures. (b) **Transparency:** Grad-CAM heatmaps validate lesion localization. (c) **Fidelity:** Segmentation masks show high overlap with ground truth.

4.3 Discussion

Our results highlight the efficacy of integrating diverse inductive biases within a hierarchical decision framework. The Weighted DERNet effectively resolves the sensitivity-specificity trade-off by fusing EfficientNetV2-S's high specificity with ResNet50's robust recall, establishing a clinical equilibrium superior to single-stream baselines. regarding localization, the CSP-Darknet backbone demonstrates superior feature preservation compared to explicit edge priors (e.g., EGCA-Net), evidenced by a +11.65% AP gain in detecting subtle Foraminal Stenosis. Crucially, the pipeline functions as a conditional hard-attention gate; by leveraging high-specificity screening (81.68%) to preemptively filter normal studies, we significantly mitigate detector false positives, driving the system-wide mAP@0.5 to 40.10%.

5 Conclusion

This study addressed the critical bottleneck in automated spinal analysis: the trade-off between high-sensitivity screening and the precise localization of subtle pathologies. By synergizing a probabilistic DERNet ensemble with a specialized YOLO11-L detector, we successfully established a unified framework that overcomes severe class imbalance without compromising diagnostic precision. Empirical validation on the VinDr-SpineXR benchmark confirms that exploiting architectural heterogeneity significantly enhances triage performance (AUROC

91.03%), while the optimized CSP-Darknet backbone proves essential for resolving minute lesions like Foraminal Stenosis (mAP@0.5 40.10%). Beyond algorithmic advancements, the successful deployment of our ONNX-integrated web interface bridges the translational gap, offering a scalable, low-latency solution to augment radiologist decision-making in real-world clinical workflows.

References

1. Cheng, L.W., Chou, H.H., Cai, Y.X., et al.: Automated detection of vertebral fractures from x-ray images: A novel machine learning model and survey of the field. Neurocomputing **566**, 126946 (2024)
2. Guo, L., Peng, B., Lei, J., Zhang, X., Zhao, J., Huang, Q.: Spinal lesion detection in X-Ray images via edge guidance and context aggregation. IEEE Transactions on Instrumentation and Measurement **74**, 1–11 (2025). https://doi.org/10.1109/TIM.2025.3527484
3. He, K., Zhang, X., Ren, S., Sun, J.: Deep residual learning for image recognition. In: Proceedings of the IEEE conference on computer vision and pattern recognition. pp. 770–778 (2016)
4. Huang, G., Liu, Z., Van Der Maaten, L., Weinberger, K.Q.: Densely connected convolutional networks. In: Proceedings of the IEEE conference on computer vision and pattern recognition. pp. 4700–4708 (2017)
5. Huang, J., Zhu, X., Chen, Z., Lin, G., Huang, M., Feng, Q.: Pathological priors inspired network for vertebral osteophytes recognition. IEEE Transactions on Medical Imaging **43**(7), 2522–2536 (2024)
6. Khan, A., Gupta, S., Arsalan, M.: Healnnet-lesions: A deep learning framework for spinal lesion detection demonstrating x-ray images as a screening alternative. Preprints (2025). https://doi.org/10.20944/preprints202510.0094.v1
7. Krupinski, E.A., Berbaum, K.S., Caldwell, R., Schartz, K., Kim, J.: Long radiology workdays reduce detection and accommodation accuracy. Journal of the American College of Radiology **7**(9), 698–704 (2010)
8. Lin, T.Y., Goyal, P., Girshick, R., He, K., Dollár, P.: Focal loss for dense object detection. In: Proceedings of the IEEE international conference on computer vision. pp. 2980–2988 (2017)
9. Nguyen, H.T., Pham, H.H., Nguyen, N.T., Nguyen, H.Q., Huynh, T.Q., Dao, M., Vu, V.: Vindr-spinexr: A deep learning framework for spinal lesions detection and classification from radiographs. In: International Conference on Medical Image Computing and Computer-Assisted Intervention. pp. 291–301. Springer (2021)
10. Pham, H.H., Nguyen Trung, H., Nguyen, H.Q.: VinDr-SpineXR: A large annotated medical image dataset for spinal lesions detection and classification from radiographs. PhysioNet (Aug 2021). https://doi.org/10.13026/q45h-5h59, https://doi.org/10.13026/q45h-5h59, version 1.0.0
11. Pinto, A., Berritto, D., Russo, A., Riccitiello, F., Caruso, M., Belfiore, M.P., Papapietro, V.R., Carotti, M., Pinto, F., Giovagnoni, A., et al.: Traumatic fractures in adults: missed diagnosis on plain radiographs in the emergency department. Acta Bio Medica: Atenei Parmensis **89**(Suppl 1), 111 (2018)
12. Priolo, F., Cerase, A.: The current role of radiography in the assessment of skeletal tumors and tumor-like lesions. European Journal of Radiology **27**, S77–S85 (1998)
13. Ren, S., He, K., Girshick, R., Sun, J.: Faster r-cnn: Towards real-time object detection with region proposal networks. Advances in neural information processing systems **28** (2015)

14. Shen, D., Wu, G., Suk, H.I.: Deep learning in medical image analysis. Annual review of biomedical engineering **19**, 221–248 (2017)
15. Sun, P., Zhang, R., Jiang, Y., Kong, T., Xu, C., Zhan, W., Tomizuka, M., Li, L., Yuan, Z., Wang, C., et al.: Sparse r-cnn: End-to-end object detection with learnable proposals. In: Proceedings of the IEEE/CVF conference on computer vision and pattern recognition. pp. 14454–14463 (2021)
16. Sutradhar, D., et al.: Cervical spine fracture detection utilizing yolov8 and deep attention-based vertebrae classification ensuring xai. Biomedical Signal Processing and Control **101**, 107228 (2025)
17. Tan, M., Le, Q.: Efficientnetv2: Smaller models and faster training. In: International conference on machine learning. pp. 10096–10106. PMLR (2021)
18. Zhang, D., Chen, B., Li, S.: Sequential conditional reinforcement learning for simultaneous vertebral body detection and segmentation with modeling the spine anatomy. Medical Image Analysis **67**, 101861 (2021). https://doi.org/10.1016/j.media.2020.101861
19. Zhang, H., Li, F., Liu, S., Zhang, L., Su, H., Zhu, J., Ni, L.M., Shum, H.: Dino: Detr with improved denoising anchor boxes for end-to-end object detection. In: International Conference on Learning Representations (ICLR). pp. 1–12 (2023)